Earth and Planetary Science Letters 478 (2017) 258–271

Contents lists available at ScienceDirect

Earth and Planetary Science Letters

www.elsevier.com/locate/epsl

Asthenospheric outflow from the shrinking Philippine Sea Plate: Evidence from Hf–Nd isotopes of southern Mariana lavas

Julia M. Ribeiro [a,*], Robert J. Stern [b], Fernando Martinez [c], Jon Woodhead [d], Min Chen [a], Yasuhiko Ohara [e,f]

[a] Rice University, Houston, TX 77005, USA
[b] University of Texas at Dallas, Richardson, TX 75080, USA
[c] SOEST, Hawai'i Institute of Geophysics and Planetology, Honolulu, HI 96822, USA
[d] The University of Melbourne, Parkville, VIC 3010, Australia
[e] Hydrographic and Oceanographic Department of Japan, Tokyo 100-8932, Japan
[f] Japan Agency for Marine-Earth Science and Technology, Yokosuka 237-0061, Japan

ARTICLE INFO

Article history:
Received 27 June 2017
Received in revised form 11 August 2017
Accepted 14 August 2017
Available online xxxx
Editor: A. Yin

Keywords:
Indian mantle
Pacific mantle
Hf–Nd isotopic systematics
Southern Marianas
subduction-driven mantle flow
Philippine Sea Plate kinematics

ABSTRACT

At subduction zones, sinking of the downgoing lithosphere is thought to enable a return flow of asthenospheric mantle around the slab edges, so that the asthenosphere from underneath the slab invades the ambient mantle flowing underneath the volcanic arc and the backarc basin. For instance at the northern end of the Lau Basin, trench retreat and slab rollback enable toroidal return flow of Samoan mantle beneath a transform margin to provide a supply of fresh, undepleted Indian mantle that feeds the backarc spreading center. Questions, however, arise about the sense of mantle flow when plate kinematics predict that the trench is advancing, as seen in the Mariana convergent margin. Does the mantle flow in or does it escape outward through slab tears or gaps? Here, we address the origin and sense of asthenospheric mantle flow supplying the southern Mariana convergent margin, a region of strong extension occurring above the subducting Pacific plate. Does the asthenosphere flow northward, from underneath the Pacific plate and Caroline hotspot through a slab tear or gap, or does it flow outward from the Mariana Trough, which possesses a characteristic Indian Ocean isotopic signature? To address these questions, we integrate geodetic data along with new Hf–Nd isotopic data for fresh basaltic lavas from three tectonic provinces in the southernmost Marianas: the Fina Nagu volcanic complex, the Malaguana–Gadao backarc spreading ridge and the SE Mariana forearc rift. Our results indicate that Indian mantle flows outward and likely escapes through slab tears or gaps to accommodate shrinking of the Philippine Sea plate. We thus predict that asthenospheric flow around the Pacific slab at the southern Mariana Trench is opposite to that predicted by most subduction-driven mantle flow models.

1. Introduction

Convection of asthenospheric mantle is thought to be mainly driven by the motions of the lithospheric plates on Earth. Asthenosphere and lithosphere are viscously coupled, so that the oceanic plate entrains the underlying mantle as it is pulled away from the spreading center. As the plate sinks at subduction zones, the overlying mantle is dragged down with the slab, inducing convection of asthenospheric mantle (Conrad and Lithgow-Bertelloni, 2002). Three-dimensional fluid-dynamic experiments have thus proposed that the flow of asthenospheric mantle is driven by the motion of the descending plate (e.g., Kincaid and Griffiths, 2003; Schellart et al., 2007; Strak and Schellart, 2014), so that they consider the *local* mantle flow that is induced by proximal plate motion. In such models, the descending plate acts as a barrier to lateral mantle flows, and tears or gaps in the plunging plate enable a return flow (toroidal inflow) of asthenospheric mantle around the slab edges (e.g., Govers and Wortel, 2005; Kincaid and Griffiths, 2003; Millen and Hamburger, 1998; Strak and Schellart, 2014). However, asthenospheric flow may also accommodate volumetric variations of shrinking or growing oceanic plates (Alvarez, 1982, 2001). Such a *regional-scale* mantle flow depends on the kinematics of entire plates and their interactions with adjacent plates (i.e., convergence zone, transform fault, or extension zone), which controls whether asthenosphere flows inward (i.e., growing plate) or outward (i.e., shrinking plate). For instance, Australia is a growing plate where

* Corresponding author.
E-mail address: juliaribeiro@rice.edu (J.M. Ribeiro).

http://dx.doi.org/10.1016/j.epsl.2017.08.022
0012-821X/

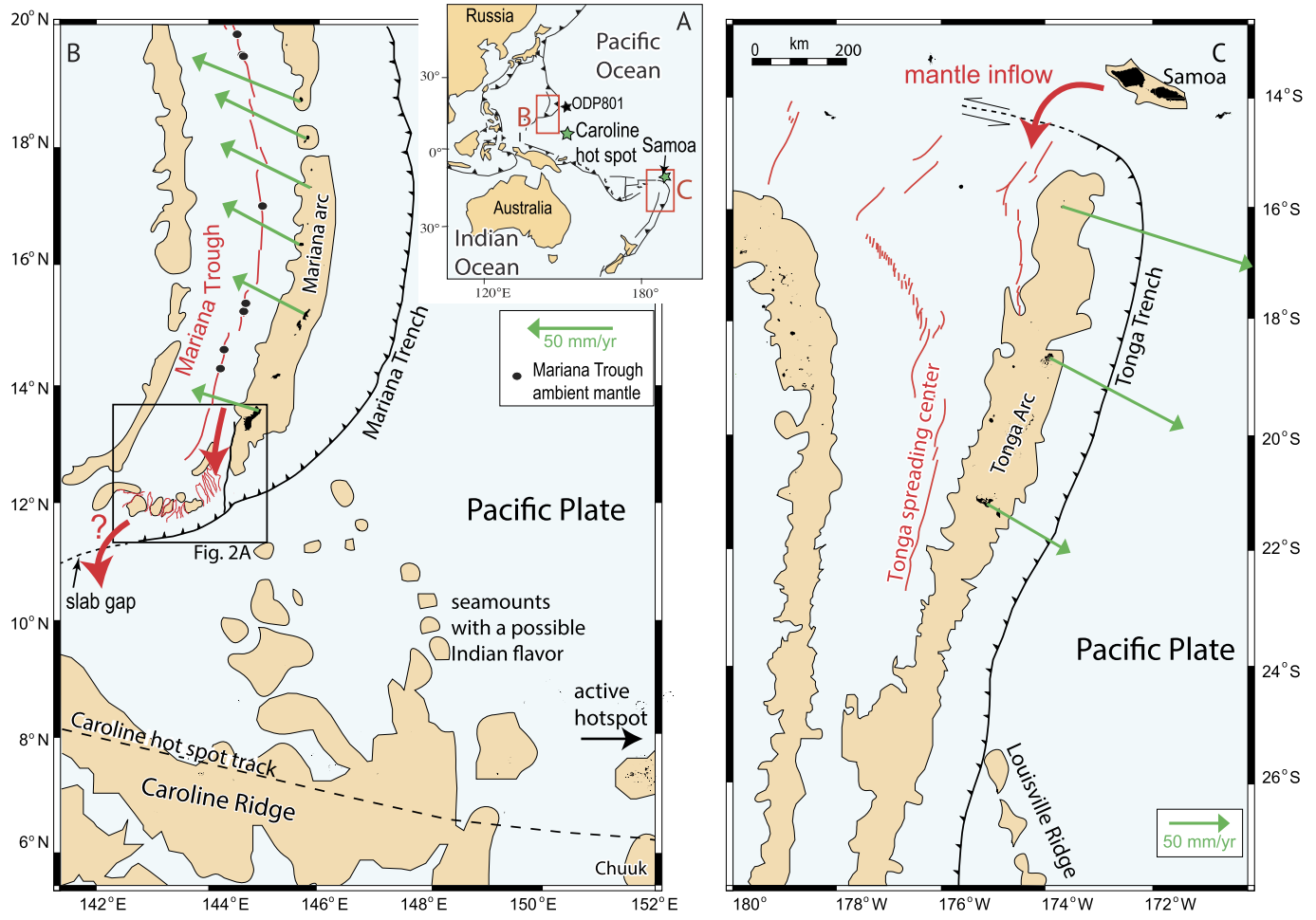

Fig. 1. A) Location map. Red boxes in A show the expanded area shown in B and C. B) Map of the southern Mariana convergent margin showing the Caroline Ridge and associated seamounts. Chuuk represents one of the Caroline hotspot volcanoes. Red lines show the backarc basin spreading centers. Location of places on the spreading ridge where the Mariana Trough ambient mantle was identified is depicted as black circles. Black box show the expanded area of Fig. 2A. The GPS vectors (green arrows) of the Mariana island stations with respect to stable Eurasia demonstrate that the Mariana Trench is advancing (Kato et al., 2003). The southwestern edge of the Pacific plate at ~142°E may allow a gap (Hayes et al., 2012) where asthenosphere can flow (thick red arrows). C) Map of the northern Tonga and Samoa seamount. Pacific mantle from underneath Samoa invades the Indian mantle flowing in Tonga. The GPS vectors of the Tonga Ridge island stations with respect to Australia indicate that the Tonga Trench is rolling back. (For interpretation of the references to color in this figure legend, the reader is referred to the web version of this article.)

local-scale mantle-flow models and regional-scale plate kinematics both predict an inflow of asthenosphere along the northern end of the Tonga Trench (Dvorkin et al., 1993; Govers and Wortel, 2005). The retrograde motion of the Tonga Trench (Dvorkin et al., 1993) is thus thought to induce toroidal (lateral) inflow of Samoan mantle to invade the Lau backarc Basin around the torn edge of the subducted Pacific plate (Millen and Hamburger, 1998), as supported by geochemical studies and radiogenic isotopes (Caulfield et al., 2012; Pearce et al., 1999; Turner and Hawkesworth, 1998) (Fig. 1C). Local slab-induced mantle flow models also predict an inward (i.e., from underneath the Pacific plate towards the Philippine Sea) toroidal flow of asthenospheric mantle through tears and gaps in the Pacific plate subducting at the Mariana convergent margin (Fig. 1B) (e.g., Fryer et al., 2003; Govers and Wortel, 2005; Gvirtzman and Stern, 2004; Schellart et al., 2007). However, regional plate kinematics indicate advance of the Izu-Bonin–Mariana (IBM) trenches towards Eurasia (Carlson and Melia, 1984; Carlson and Mortera-Gutiérrez, 1990), predicting outflow of asthenospheric mantle around slab gaps to accommodate shrinking of the Philippine Sea plate (PSP) (Alvarez, 1982, 2001; Kobayashi, 2004). Such contradictory interpretations thus raise the question of do regional plate kinematics or local slab–mantle interactions determine the mantle flow in or out through slab gaps or tears?

To address this issue, here we examine the flow of asthenospheric mantle in the southern Mariana margin. For this purpose, we consider the Philippine Sea plate and Mariana plate as extending to the Izu-Bonin–Mariana (IBM), Yap and Palau Trenches (Fig. 1A), which represent natural boundaries to asthenosphere flow. To the east, the Pacific trenches are advancing towards Eurasia (Kato et al., 2003) (Fig. 1B), resulting in a shrinking PSP that squeezes out the underlying asthenospheric mantle (Fig. 1A–B). A slab tear or a gap in the subducting Pacific plate (Kobayashi, 2004; Sato et al., 1997) may enable mantle outflow in the southern Marianas (Fig. 1B, 2D), implying that the asthenosphere may flow in the opposite sense as usually predicted by local subduction-driven mantle flow models (Govers and Wortel, 2005; Schellart et al., 2007; Strak and Schellart, 2014). Such mantle outflow could thus be responsible for forearc rifting and rapid slab rollback in the southern Marianas, where young oceanic crust extends from the backarc to the forearc region (Ribeiro et al., 2013a, 2013b).

Here, we investigate the origin, the nature, and the direction of the asthenospheric mantle flowing underneath PSP and Marianas (i) by reporting new Hf–Nd isotopic ratios of basaltic lavas from the southern Marianas; and (ii) by examining the net area variations of PSP, along with published geodetic data, which indicate a westward trench advance (Kato et al., 2003). Using recently com-

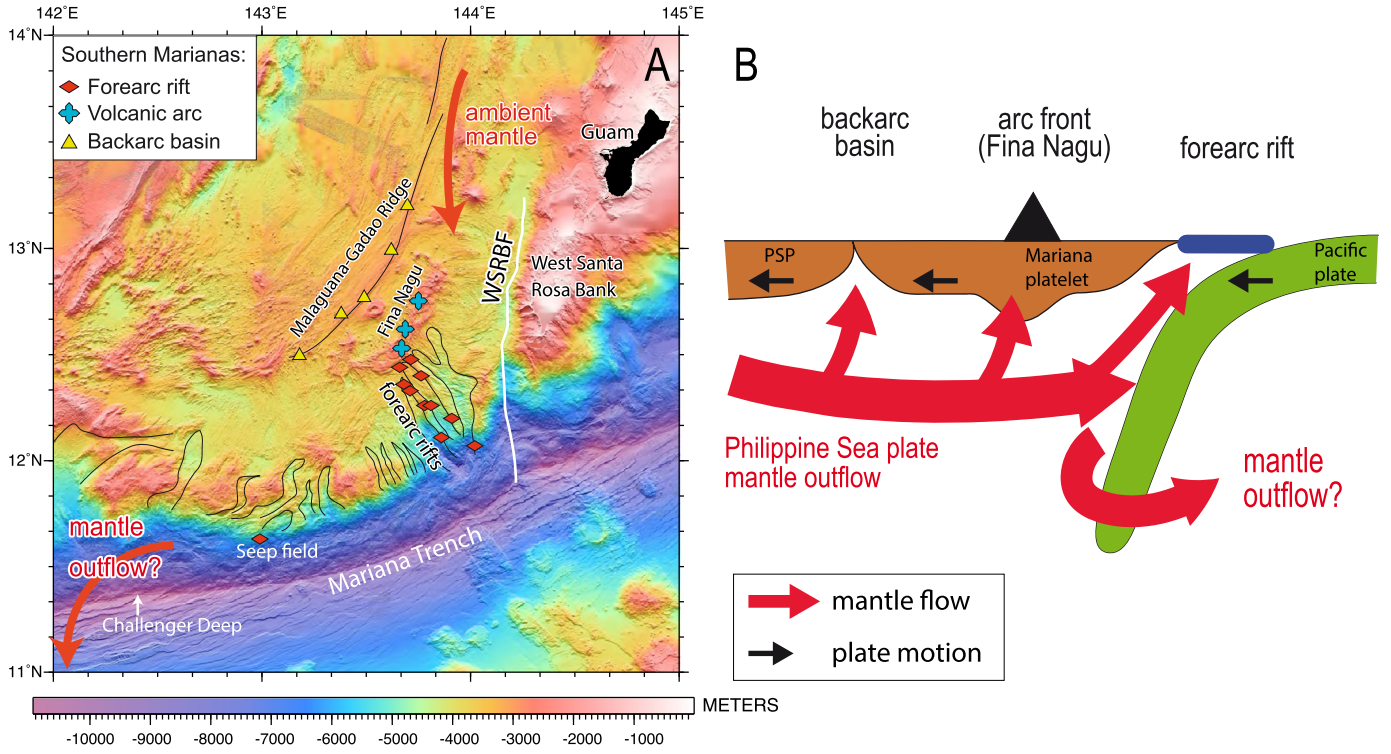

Fig. 2. A) Bathymetric map of the southern Mariana convergent margin and sample locations. The thick red arrows depict the possible mantle flows investigated in this study. The West Santa Rosa Bank Fault (WSRBF) is thought to represent the surface expression of a slab tear. B) Sketch illustrating the possible scenario occurring beneath the southern Marianas. The Mariana Trough ambient mantle flows southward and invades the southern Marianas; and then escape through the slab tears or gaps. (For interpretation of the references to color in this figure legend, the reader is referred to the web version of this article.)

piled earthquake locations, we also infer the occurrence of a slab gap along the southwestern tip of the Mariana Trench; and we show that the Indian asthenospheric mantle flowing underneath the PSP and Mariana Trough feeds the southern Mariana lavas. Our results imply that the mantle flows regionally outward from underneath the shrinking PSP and escapes through slab tears or gaps.

2. Tectonics and magmatism of the Philippine Sea plate and the Southern Marianas

The Philippine Sea plate is an oceanic plate that is mostly bounded by trenches, which include the Izu-Bonin–Mariana Trench to the east. To the west, PSP sinks underneath Eurasia at the Ryukyu and Philippine Trenches, and at the Nankai Trough to the north. A subduction polarity reversal occurs at the Manila Trench, where the Eurasian plate subducts beneath the PSP (Roeder, 1977; Suppe, 1984), so that in this area the PSP is not shrinking. Opening of the West Philippine, Parece Vela, Palau and Shikoku basins resulted in PSP growth for much of the past 50 Ma, but seafloor spreading stopped around 15 Ma (Okino et al., 1999); and since then, the PSP has shrunk. More recently, the Mariana Trough began forming by seafloor spreading at ~5 to 10 Ma (Hussong and Uyeda, 1982), and continues opening. However, Mariana Trough opening does not overcome the overall area loss due to the advance of the IBM trenches towards Eurasia (Kato et al., 2003), associated with the western subduction of PSP, which has resulted in the progressive shrinking of PSP over the past 15 Ma.

The southern portion of the Mariana intraoceanic arc marks the southern end of the ~2800-km long Izu-Bonin–Mariana convergent plate margin (Fig. 1A), where the Pacific plate plunges steeply beneath the Mariana and Philippine Sea plates at ~3 cm/yr (Bird, 2003). Opening of the Mariana Trough is now most vigorous in the extreme south. The southern Mariana Trough includes a robust backarc spreading ridge (known as the Malaguana–Gadao Ridge), a disrupted volcanic arc, and the SE Mariana forearc rift (SEMFR in Fig. 1) (Ribeiro et al., 2013a, 2013b). SEMFR erupted backarc-like tholeiitic pillow lavas and massive flows unusually close (<80 km) to the trench in Pliocene time (i.e., ^{40}Ar–^{39}Ar age of 3.8 to 2.7 Ma) (Ribeiro et al., 2013b). Opening of the backarc basin also disrupted the volcanic arc front, forming a string of small volcanoes known as the Fina Nagu Volcanic Complex (FNVC in Fig. 1; Brounce et al., 2016) and the Alphabet seamounts (Stern et al., 2013). Stretching of the forearc has also enabled the formation of a low-temperature, serpentinite-hosted vent field, called the Shinkai Seep Field (Fig. 1B; Ohara et al., 2012). Some tholeiitic basaltic fragments with similar composition to the forearc rift lavas were sampled ~7.5 km west of the Shinkai Seep Field (Ohara et al., 2012; Stern et al., 2014), suggesting that forearc rifting affects regions to the southwest (Ribeiro et al., 2013b). We are only beginning to understand how extension of the southern Mariana Trough occurs and how strain is distributed in this region. The occurrence of oceanic crust so close to the trench implies that fresh, hot asthenosphere has invaded the forearc (Ribeiro et al., 2013b), which is usually underlain by cold serpentinized mantle (Fryer et al., 1995; Hyndman and Peacock, 2003; Ohara and Ishii, 1998). Below, we explore the origin of this invading asthenosphere in the southernmost Mariana convergent margin.

3. Sample selection and analytical methods

Twenty samples were selected from the major magmatic subprovinces of the southern Marianas including the backarc spreading ridge (Malaguano–Gadao Ridge), the disrupted arc (Fina Nagu Volcanic Complex), SE Mariana forearc rift (SEMFR), and a rift-related occurrence near the Shinkai Seep (Fig. 2). Analyses presented here include both *in situ* microanalysis of pillow glass and bulk analyses of rock powders made from unaltered pillow interiors. These samples range from basalts to andesites. Most samples

are somewhat fractionated, as indicated by magnesium number Mg# (atomic Mg × 100/[Fe + Mg]) < 65, although two SEMFR samples are primitive (Mg# > 65). The sample suite encompasses a range in Nb/Yb from 0.3 to 1.5 in order to capture the range of enriched (high Nb/Yb) vs. depleted (low Nb/Yb) mantle variations in Hf–Nd isotopic ratios, which is, in turn, likely to capture at least two of any mixing end-members of the Mariana pre-subduction mantle array defined by Woodhead et al. (2012).

Pb–Sr–Nd–Hf isotopic analyses were conducted at the University of Melbourne using a Nu Instruments multi-collector inductively-coupled plasma mass spectrometer (ICP-MS) with sample uptake via a CETAC Aridus desolvating nebulizer. Total blanks measured during the course of this study are negligible in all cases (<20 pg), and no blank corrections were thus performed. Instrumental mass bias is corrected by normalizing to $^{146}Nd/^{145}Nd = 2.0719425$ (equivalent to $^{146}Nd/^{144}Nd = 0.7219$), $^{86}Sr/^{88}Sr = 0.1194$, and $^{179}Hf/^{177}Hf = 0.7325$ using an exponential law (Maas et al., 2005; Woodhead et al., 2001). All data are routinely normalized to primary reference materials run concurrently (La Jolla Nd = 0.511860, SRM987 Sr = 0.710230, and JMC 475 Hf = 0.282160). Uncertainties for individual analyses are $2\sigma \times 10^{-5}$ (standard error of the mean). Details are provided in the appendices and in the supplementary Table A1. Isotopic compositions of Hf, Nd, Pb and Sr isotopic ratios are reported in Table 1, along with selected major element compositions and trace element ratios.

4. Composition of the southern Mariana lavas

The major and trace element contents of the samples analyzed here are reported elsewhere (Brounce et al., 2014, 2016; Ribeiro et al., 2013a, 2013b; Stern et al., 2014); and below, we only provide a short description of the samples that summarizes their main compositional characteristics.

The southern Mariana lavas are low-K to medium-K (K_2O < 1 wt%) basalts to andesites (SiO_2 < 60 wt%; major element analyses are adjusted to 100% total on anhydrous basis) (Ribeiro et al., 2013a, 2013b). Samples from the Southern Mariana backarc are slightly more fractionated, with an andesitic composition in the diagram of Peccerillo and Taylor (1976) (Fig. 3A). The rare earth element (REE) patterns of the arc and forearc lavas range between N-MORB-like, LREE-depleted to flat patterns (Fig. 3B) with the exception of one sample that is enriched in light REE (LREE). The lavas are enriched in large ion lithophile elements (LILE; i.e., Rb, Cs, Pb, Ba, Sr, K, U) and depleted in high field strength elements (HFSE; i.e., Nb, Ta, Hf, Zr, Ti), consistent with the addition of slab fluids to their mantle source during petrogenesis (Fig. 3C). Forearc lavas display the highest LILE contents, implying a greater contribution of aqueous slab–fluids at shallow slab depths (≤80 km) (Ribeiro et al., 2013a, 2015). The southern Mariana backarc lavas have a peculiar chemical fingerprint, with flat to MREE-enriched ("humped") REE patterns and a europium anomaly, characteristic of plagioclase fractionation. They are generally more enriched in medium REE (MREE) and heavy REE (HREE), consistent with their higher degree of fractionation. They also display higher HFSE contents, especially in Ti and Zr, and lower LILE contents than do the southern Mariana arc and forearc lavas, suggesting that they formed under higher degrees of mantle melting or from a less depleted mantle source metasomatized by lower extent of slab fluids. Interestingly, the southern Mariana arc lavas do not display a strong enrichment in LILE (Fig. 3C), as generally observed for the Mariana arc lavas, implying that they captured less slab-derived fluids. In general, southern Mariana igneous rocks reflect a mantle source that was affected by hydrous slab-derived fluids and minor addition of sediment melts, reflecting variable extents in mantle melting, mantle depletion, and slab–fluid contribution across the trench.

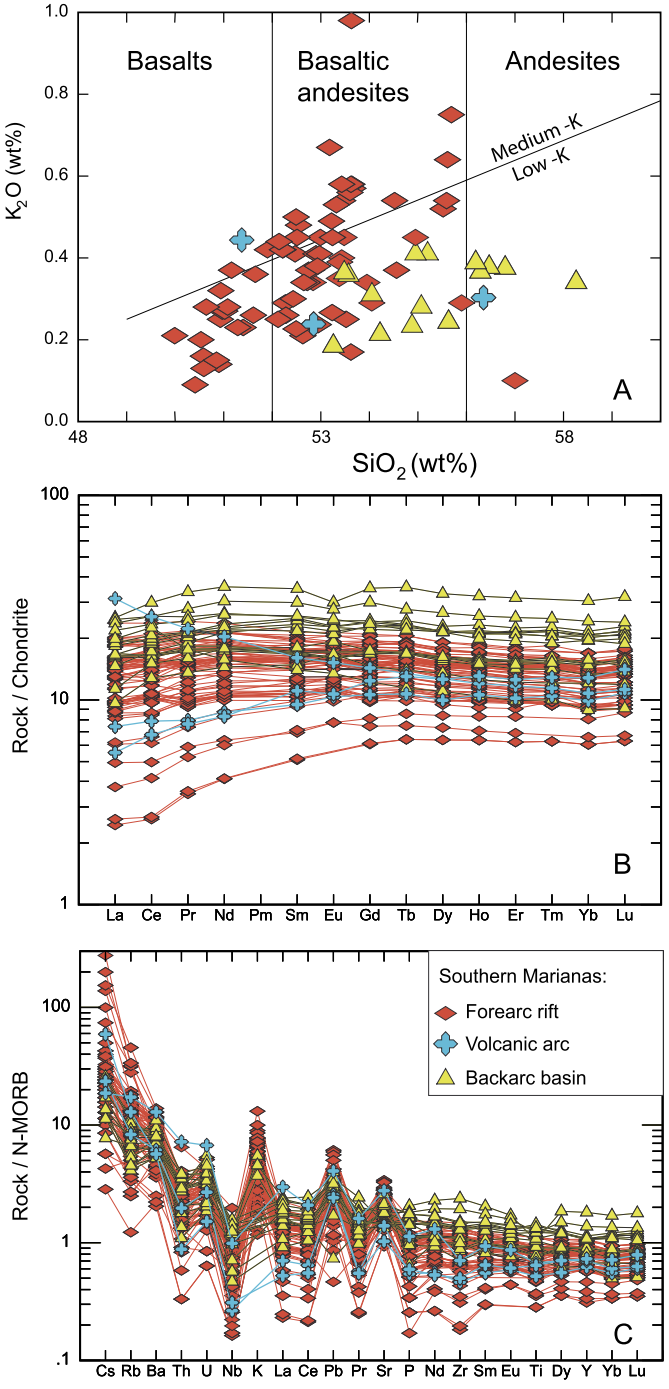

Fig. 3. Compositional characteristics of the southern Mariana lavas. A) Potassium–silica diagram of Peccerillo and Taylor (1976) showing that the lavas are basalts to andesites (adjusted to 100% anhydrous basis). B) Chondrite-normalized rare earth element (REE) patterns and C) N-MORB-normalized trace element patterns (Sun and McDonough, 1989). Lavas display LREE-depleted to flat REE patterns. Only one arc sample has LREE-enriched patterns. Lavas are enriched in LILE and depleted HFSE, consistent with their petrogenesis above a subducted plate.

5. Hf–Nd–Pb–Sr isotopic ratios

Analyzed samples from the southern Marianas have $^{143}Nd/^{144}Nd$ ratios that range from 0.51302 to 0.51315 (mean of 0.51308 ± 1), corresponding to εNd from 7.4 to 10.1 (mean of 8.7 ± 0.3). They have $^{176}Hf/^{177}Hf$ ratios that range from 0.28316 to 0.28329 (mean of 0.28321 ± 1), corresponding to εHf from 13.9 to 18.3 (mean of 15.5 ± 0.5; Fig. 3). Although a number of different Indian–Pacific boundaries in Hf–Nd space have been proposed, here we use that

Table 1
Selected major element concentrations, trace element ratios, and isotopic compositions of the southern Mariana lavas.

Cruise#	Sample	Material	ISGN	Location	Magmatic subprovince	Longitude	Latitude	SiO_2	MgO	FeO*	Mg#	$^{143}Nd/^{144}Nd$	2σ	εNd	$^{176}Hf/^{177}Hf$
TN 273	TN273-06D-01-03	glassy rind	MNB000101	spreading axis	MGR	143.49	13.77	59.82	2.15	8.59	30.85	0.513090	8	8.90	0.283211
TN 273	TN273-03W-02	glassy rind	MNB000093	spreading axis	MGR	143.70	13.20	53.72	5.24	9.62	49.26	0.513108	9	9.25	0.283240
TN 273	TN273-01D-01-01	glassy rind	MNB000097	spreading axis	MGR	143.62	14.00	56.53	2.93	9.40	35.72	0.513093	7	8.95	0.283220
TN 273	TN273-01D-01-01 (replicate)	glassy rind	MNB000097	spreading axis	MGR	143.62	14.00	56.53	2.93	9.40	35.72				
TN 273	TN273-13D-01-01	glassy rind	MNB000108	spreading axis	MGR	143.18	13.50	53.37	5.64	8.43	54.39	0.513040	8	7.92	0.283165
TN 273	TN273-08D-01-01	glassy rind	MNB000105	spreading axis	MGR	143.38	13.69	58.26	2.47	10.14	30.28	0.513076	8	8.62	0.283195
			Mean	***spreading axis***	***MGR***	***143.50***	***13.69***	***56.37***	***3.56***	***9.26***	***39.37***	***0.513081***	***2***	***8.73***	***0.283206***
TN 273	TN273-24D-01-01	glassy rind	MNB000110	volcanic arc	FNVC	143.67	12.53	57.9	2.73	10.8	31.06	0.513064	9	8.39	0.283187
TN 273	TN273-42D-01-01	glassy rind	MNB000116	volcanic arc	FNVC	143.75	12.75	51.37	6.06	10.23	51.36	0.513016	8	7.45	0.283164
TN 273	TN273-42D-01-01 (replicate)	glassy rind	MNB000116	volcanic arc	FNVC	143.75	12.75	51.37	6.06	10.23	51.36	0.513018	8	7.49	
TN 273	TN273-44D-01-01	glassy rind	MNB000117	volcanic arc	FNVC	143.68	12.62	56.35	4.4	10.22	43.42	0.513070	7	8.51	0.283178
			Mean	***volcanic arc***	***FNVC***	***143.71***	***12.66***	***54.25***	***4.81***	***10.37***	***44.30***	***0.513042***	***3***	***7.96***	***0.283176***
TN 273	TN273-22D-01-01	bulk rock	JMR000005	forearc rift	NW SEMFR	143.68	12.36	53.38	6.25	9.54	53.87	0.513073	8	8.56	0.283206
TN 273	TN273-25D-01-03	bulk rock	JMR000007	forearc rift	NW SEMFR	143.66	12.44	57.9	3.19	9.88	36.53	0.513071	8	8.52	0.283189
TN 273	TN273-29D-02-01	bulk rock	JMR00000A	forearc rift	NW SEMFR	143.72	12.48	53.39	6.64	8.41	58.46	0.513075	8	8.60	0.283209
YK10-12	YKDT88-R2	bulk rock	JMR000033	forearc rift	NW SEMFR	143.76	12.40	50.85	10.22	6.84	72.70	0.513097	8	9.03	0.283210
TN 273	TN273-20D-01-01	bulk rock	JMR000004	forearc rift	NW SEMFR	143.71	12.33	55.9	4.44	10.85	42.18	0.513072	8	8.54	0.283187
			Mean	***forearc rift***	***NW SEMFR***	***143.706***	***12.402***	***54.284***	***6.148***	***9.104***	***52.75***	***0.513078***	***1***	***8.65***	***0.283200***
TN 273	TN273-33D-01-23	bulk rock	JMR00000M	forearc rift	SE SEMFR	143.78	12.26	53.8	5.4	7.66	55.69	0.513075	8	8.60	0.283235
TN 273	TN273-19D-01-01	bulk rock	JMR000002	forearc rift	SE SEMFR	143.81	12.26	55.61	4.65	10.61	43.86	0.513063	6	8.37	0.283186
YK10-12	6K-1230-R26	bulk rock	JMR000024	forearc rift	SE SEMFR	143.91	12.20	51.90	6.54	8.38	58.18	0.513087	8	8.84	0.283229
YK10-12	6K-1235-R8	bulk rock	JMR00002C	forearc rift	SE SEMFR	144.02	12.07	53.62	6.85	7.84	60.90	0.513149	8	10.05	0.283289
YK08-08	6K-1096-R21	bulk rock	JMR00001J	forearc rift	SE SEMFR	143.86	12.11	51.61	8.13	7.21	66.78	0.513113	8	9.34	0.283250
			Mean	***forearc rift***	***SE SEMFR***	***143.88***	***12.18***	***53.31***	***6.31***	***8.34***	***57.08***	***0.513097***	***3***	***9.04***	***0.283238***
YK13-08	12541-12001-6K1363-R05	glassy rind	JMR00004B	forearc rift	Seep Field	142.99	11.63	51.00	6.17	8.23	57.20	0.513098	8	9.05	0.283223
YK13-08	12541-12001-6K1363-R06	glassy rind	JMR00004C	forearc rift	Seep Field	142.99	11.63	51.37	5.59	8.66	53.50	0.513010	6	7.33	0.283212
			Mean	***forearc rift***	***Seep Field***	***142.99***	***11.63***	***51.18***	***5.88***	***8.44***	***55.35***	***0.513054***		***8.19***	***0.283218***
			Mean		***Southern Marianas***			***54.34***	***5.21***	***9.14***	***48.79***	***0.513074***		***8.59***	***0.283209***
			2σ					*1.19*	*0.87*	*0.52*	*5.22*	*0.000015*		*0.28*	*0.000013*

MGR: Malaguana–Gadao backarc basin spreading ridge, FNVC: Fina Nagu volcanic arc chain, SEMFR: southeast Mariana forearc rift.

Table 1 (*Continued.*)

Cruise#	Sample	εHf	$^{87}Sr/^{86}Sr$	2σ	$^{206/204}Pb$	$^{207/204}Pb$	$^{208/204}Pb$	Nb/Yb	Hf/Sm	Th/Ta	Ba/Th	Ba/Nb	References for major and trace elements
TN 273	TN273-06D-01-03	15.52	0.703004	17	18.419	15.488	38.013	1.01	0.86	2.01	91.60	11.79	Brounce et al. (2014)
TN 273	TN273-03W-02	16.55	0.702958	19	18.559	15.501	38.158	0.49	0.63	1.98	269.58	33.2	Brounce et al. (2014)
TN 273	TN273-01D-01-01	15.84	0.702978	18	18.504	15.504	38.100	1.49	0.76	1.72	126.15	11.03	Brounce et al. (2014)
TN 273	TN273-01D-01-01 (replicate)				18.506	15.508							Brounce et al. (2014)
TN 273	TN273-13D-01-01	13.90	0.703179	20	18.923	15.563	38.443	1.09	0.71	5.90	149.45	41.804	Brounce et al. (2014)
TN 273	TN273-08D-01-01	14.96	0.703069	20	18.774	15.530	38.280	0.84	0.77	2.39	118.46	19.56	Brounce et al. (2014)
		15.36	***0.703038***	***8***	***18.614***	***15.516***	***38.184***	***0.98***	***0.75***	***2.80***	***151.05***	***23.48***	
TN 273	TN273-24D-01-01	14.68	0.703302	20	19.024	15.567	38.525	0.37	0.71	163.24	62.47		Brounce et al. (2016)
TN 273	TN273-42D-01-01	13.86	0.703116	20	19.040	15.563	38.527	1.25	0.57	6.56	94.16	35.36	Brounce et al. (2016)
TN 273	TN273-42D-01-01 (replicate)												Brounce et al. (2016)
TN 273	TN273-44D-01-01	14.36	0.703233	18	18.985	15.566	38.513	0.33	0.66	2.85	338.17	49.48	Brounce et al. (2016)
		14.30	***0.703217***	***11***	***19.016***	***15.565***	***38.522***	***0.65***	***0.65***	***4.70***	***198.52***	***49.10***	
TN 273	TN273-22D-01-01	15.35	0.703429	19	18.810	15.553	38.334	0.30	0.69	3.42	266.18	63.63	Ribeiro et al. (2013a)
TN 273	TN273-25D-01-03	14.75	0.703336	19	19.017	15.559	38.496	0.59	0.78	3.14	209.32	43.02	Ribeiro et al. (2013a)
TN 273	TN273-29D-02-01	15.45	0.703402	19	18.860	15.544	38.382	0.53	0.75	2.41	253.22	43.46	Ribeiro et al. (2013a)
YK10-12	YKDT88-R2	15.49	0.703218	18	18.915	15.545	38.408	0.37	0.64	1.41	354.58	37.33	Ribeiro et al. (2013b)
TN 273	TN273-20D-01-01	14.68	0.703322	19	18.914	15.547	38.412	0.57	0.72	3.47	184.24	36.67	Ribeiro et al. (2013a)
		15.14	***0.703341***	***7***	***18.903***	***15.550***	***38.406***	***0.472***	***0.72***	***2.77***	***253.51***	***44.82***	
TN 273	TN273-33D-01-23	16.37	0.703288	19	18.828	15.564	38.361	0.78	0.74	7.74	93.42	48.72	Ribeiro et al. (2013a)
TN 273	TN273-19D-01-01	14.64	0.703349	19	19.020	15.554	38.487	0.54	0.73	2.52	262.66	42.94	Ribeiro et al. (2013a)
YK10-12	6K-1230-R26	16.16	0.703148	15	18.654	15.538	38.278	1.17	0.73	2.35	142.41	21.79	Ribeiro et al. (2013b)
YK10-12	6K-1235-R8	18.28	0.703277	13	18.466	15.525	38.131	1.37	0.70	1.02	139.68	9.52	Ribeiro et al. (2013b)
YK08-08	6K-1096-R21	16.90	0.703205	19	18.702	15.547	38.328	0.66	0.65	2.21	271.38	43.04	Ribeiro et al. (2013b)
		16.47	***0.703253***	***7***	***18.734***	***15.546***	***38.317***	***0.90***	***0.71***	***3.17***	***181.91***	***33.20***	
YK13-08	12541-12001-6K1363-R05	15.95	0.702988	14	18.555	15.512	38.156	1.16	0.64	1.75	148.57	15.35	Stern et al. (2014)
YK13-08	12541-12001-6K1363-R06	15.56	0.702982	16	18.544	15.511	38.155	1.13	0.71	1.59	151.48	14.98	Stern et al. (2014)
		15.75	***0.702985***	***1***	***18.550***	***15.512***	***38.156***	***1.14***	***0.68***	***1.67***	***150.02***	***15.16***	
		15.46	***0.703189***		***18.763***	***15.538***	***38.314***	***0.80***	***0.71***	***2.97***	***191.40***	***34.26***	
		0.47	*0.000068*		*0.090*	*0.011*	*0.069*	*0.16*	*0.03*	*0.79*	*35.43*	*7.25*	

of Pearce et al. (1999) to define the mantle domains in the southern Marianas (Supplementary Fig. C1) for consistency with other recent studies (e.g., Miyazaki et al., 2015). All samples plot in the Indian Ocean domain on the Nd–Hf isotope diagram of Pearce et al. (1999). Our data define a trend that plots on the right side of the compositional spectrum of the Mariana backarc basin lavas, closer to the Pacific mantle domain relative to most analyses of the modern Mariana arc and backarc basin lavas (Fig. 4A). They show much less variation than other Mariana Trough lavas.

The southern Mariana lavas display $^{87}Sr/^{86}Sr$ that range from 0.70298 to 0.70343 (mean of 0.70319±7) (Fig. 4B). The Pb isotopic compositions of the southern Mariana forearc lavas encompass the field of Mariana backarc lavas (mean $^{206}Pb/^{204}Pb = 18.76 \pm 0.09$, $^{208}Pb/^{204}Pb = 38.31 \pm 0.07$, $^{207}Pb/^{204}Pb = 15.54 \pm 0.01$) (Fig. 4C). FNVC lavas are generally more radiogenic in Pb, with a mean of 19.02 ± 0.03 for $^{206}Pb/^{204}Pb$, 38.52 ± 0.01 for $^{208}Pb/^{204}Pb$, and 15.57 ± 0.01 for $^{207}Pb/^{204}Pb$, indicating that the volcanic arc captured a higher extent of subduction input than the rest of the southern Mariana lavas (Ribeiro et al., 2013a, 2015).

6. A shrinking Philippine Sea plate

Early models of backarc basin formation generally assumed gravitationally driven foundering of slabs within a passive mantle, leading to retrograde rollback of the subduction hinge relative to the mantle (Elsasser, 1971; Molnar and Atwater, 1978). Following on these studies, several geologic and geodynamic models proposed toroidal inflow of asthenospheric mantle around the edges of the subducted Pacific plate along the IBM trench (e.g., Fryer et al., 2003; Govers and Wortel, 2005; Gvirtzman and Stern, 2004; Schellart et al., 2007) (Fig. 1B). Nevertheless, it has long been recognized that the IBM system is advancing toward Eurasia following the WNW motion of the Philippine Sea plate (Carlson and Melia, 1984; Carlson and Mortera-Gutiérrez, 1990). Subsequent geodetic studies confirm and refine rates of westward trench advance (Kato et al., 2003), implying shrinking of the Philippine Sea plate and outflow of underlying asthenospheric mantle. To further assess the implications of these kinematic models, we here use geodetic data (Kato et al., 2003) to determine the current rate of change in size of the Philippine Sea plate, and examine the distribution of slabs and associated slab gaps around the plate to evaluate possible avenues of mantle outflow.

To estimate the rate of change of the Philippine Sea plate area, we define it by the major surrounding trenches and the Ayu Trough axis at the southern end. We then account for plate area consumption along the western trenches and growth due to backarc spreading (i.e., Mariana Trough). The Philippine Sea plate, with an area A_P of $\sim 5.61 \times 10^6$ km^2, is associated with the smaller ($\sim 0.50 \times 10^6$ km^2) Mariana plate (Bird, 2003) to the east. PSP moves northwestward with respect to Eurasia at variable rates, from ~57 to 101 km/Myr, given by the Eu–Ph Euler pole (61.4°N, 163.7°E, 1°/Myr) (Kato et al., 2003) (Fig. 5A). The westward motion of the Philippine Sea plate is accommodated by subduction along the Nankai, Ryukyu, and Philippine Trenches, and eastward subduction of the Eurasian plate at the Manila Trench, which does not affect PSP area. The Pacific trenches are thus moving WNW at about the same convergence rate as PSP, as depicted by the thin white flow lines in Fig. 5A. The exception is the Mariana Trench, which lags the Philippine Sea plate motion leading to the opening of the Mariana Trough (Kato et al., 2003).

Using the small circle convergence rates of the Philippine Sea plate (thin white lines and associated numbers in Fig. 5A), we can estimate the shrinking rate S (km^2/Myr) of PSP by integrating these convergence rates u (mm/yr) against the great circle distance from the opening pole x (km), such as

$$dS = u\,dx \qquad (1)$$

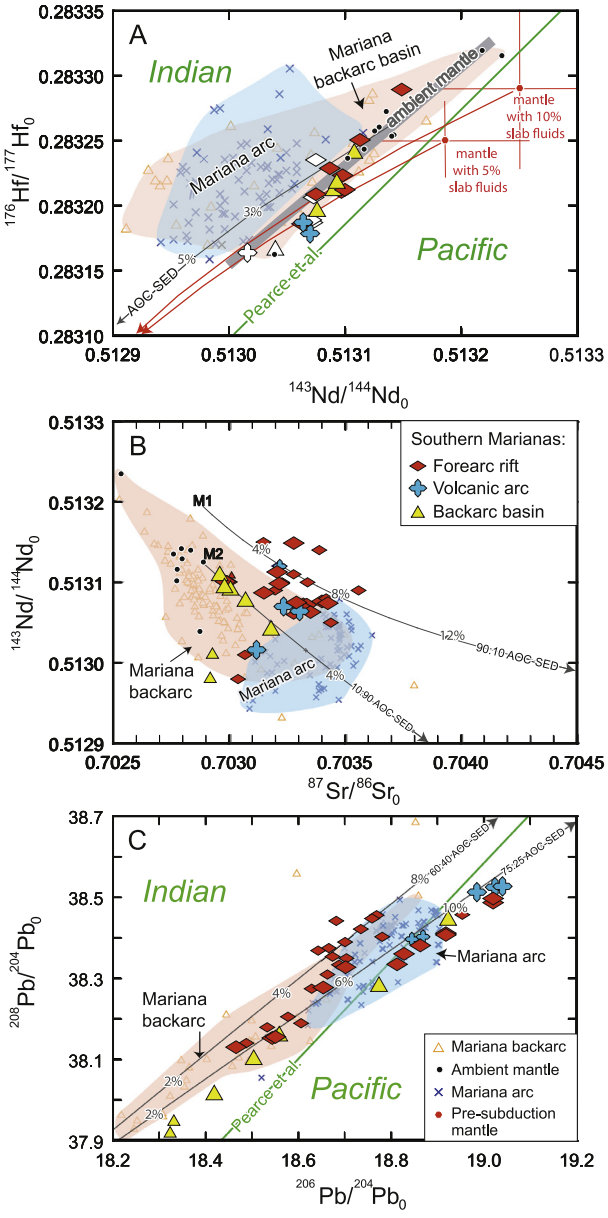

Fig. 4. Age-corrected Nd–Hf–Sr–Pb systematics for the southern Mariana lavas. A) Hf–Nd diagram used to highlight mantle heterogeneities beneath the southern Marianas. The southern Mariana lavas display similar Hf–Nd composition to that of the Mariana Trough lavas, suggesting that Indian-type mantle flowed from the Mariana Trough to the south. Southern Mariana samples filtered for Th/Ta <3 are depicted as filled symbols, and lavas with Th/Ta >3 are represented as opened symbols (samples are filtered only in panel A). The Hf–Nd isotopic composition of the Mariana arc lavas is explained as a mixing array between the ambient mantle and a 60: 40 bulk mixture between the downgoing altered oceanic crust and overlying sediments (ODP, Site 801) as in Woodhead et al. (2012) (thin black line entitled "AOC-SED"). The red diamonds entitled "mantle with 10% slab fluids" and "mantle with 5% slab fluids" represent an averaged composition of pre-subduction mantle (i.e., prior to any slab fluid addition), which was reconstructed using Eq. (6). Error bars are one standard deviation (1σ) to the mean. We used the same slab fluid composition as for the Mariana arc lavas in Eq. (6). B) $^{143}Nd/^{144}Nd$ vs. $^{87}Sr/^{86}Sr$ diagram. C) $^{208}Pb/^{204}Pb$ vs $^{206}Pb/^{204}Pb$ diagram. The mixing arrays assume bulk mixtures. Larger symbols for the southern Mariana lavas represent data reported in this study; and smaller symbols report data that were analyzed by Ribeiro et al. (2013a). Analytical uncertainties are smaller than are the symbols. The thick green line represents the geochemical boundary between Pacific and Indian mantle domains of Pearce et al. (1999). M1 and M2 represent the end-member composition of the depleted mantle. Details can be found in appendix D and in supplementary Tables B1-2 and B1-3. (For interpretation of the references to color in this figure legend, the reader is referred to the web version of this article.)

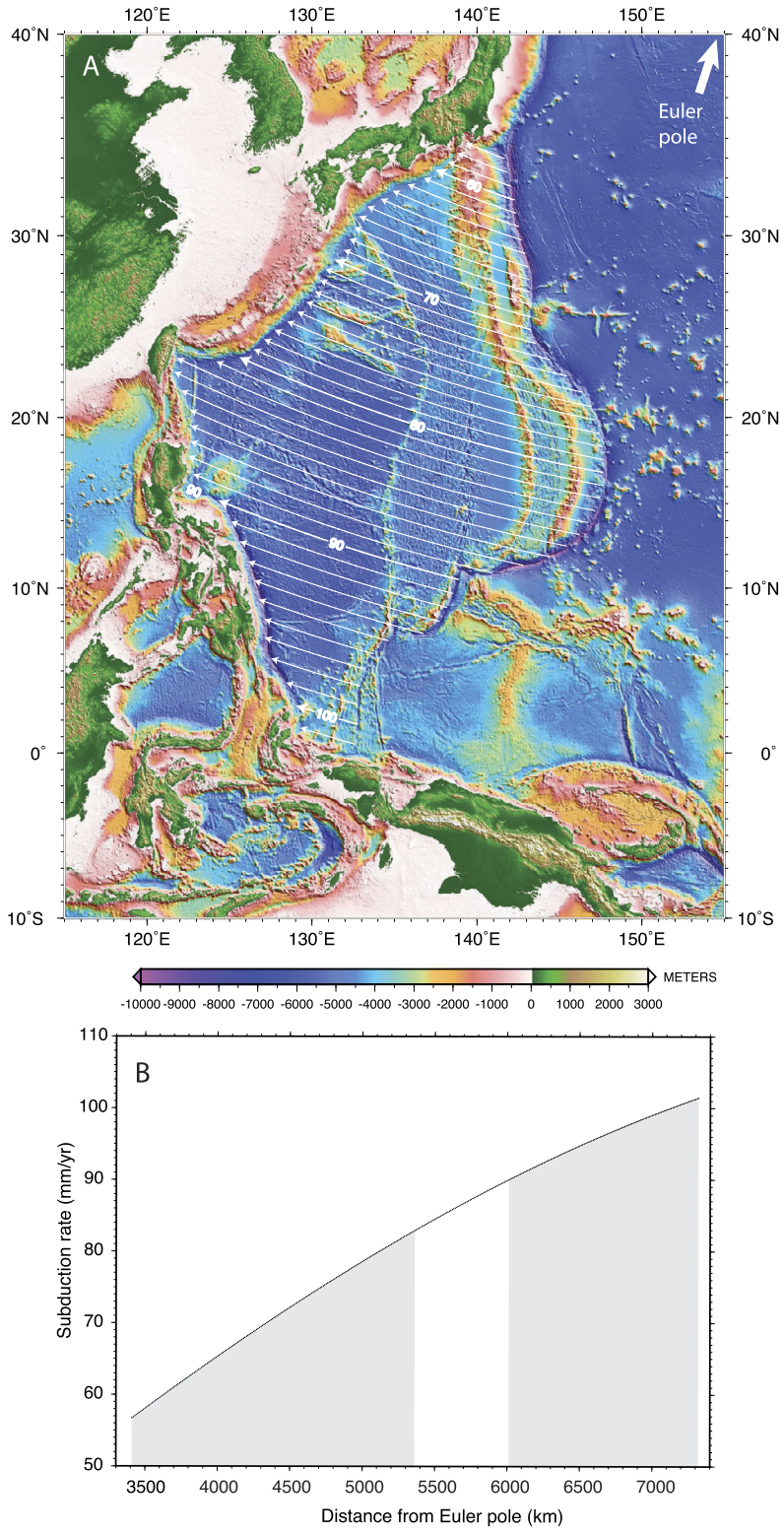

Fig. 5. Figures illustrating the shrinking of the Philippine Sea Plate. A) Bathymetric map of the Philippine Sea plate showing the flow lines (thin white lines) and the convergence rates (numbers in mm/yr) with respect to Eurasia using the pole of Kato et al. (2003) (61.4°N, 163.7°E, 1°/Ma). IBM trench is migrating WNW with respect to a relatively stable Eurasia, so that PSP is shrinking. B) Plot showing the variation of the convergence rates with great circle distance from the opening pole used in our calculations. The rate of the plate motion along small circles was integrated against distance from the opening pole every 10 km. The gray area represents the shrinkage rate. The white area represents the Manila Trench section where PSP is not subducting and is therefore excluded from our area-rate calculations. We separately estimate the Mariana Trough growth rate as described in the text and remove this from the PSP shrinkage rate. We find that PSP is shrinking at about 0.21 km^2/yr.

We find a shrinking rate of about 264.7×10^3 km^2/Myr for PSP. For simplification, we consider that the change in area of PSP is primarily due to subduction, and that shortening associated with collision zones (e.g., Taiwan) and subduction reversal at the Manila Trench do not affect Philippine Sea plate area (Fig. 5B). The Mariana Trench is lagging behind PSP, resulting in opening of the Mari-

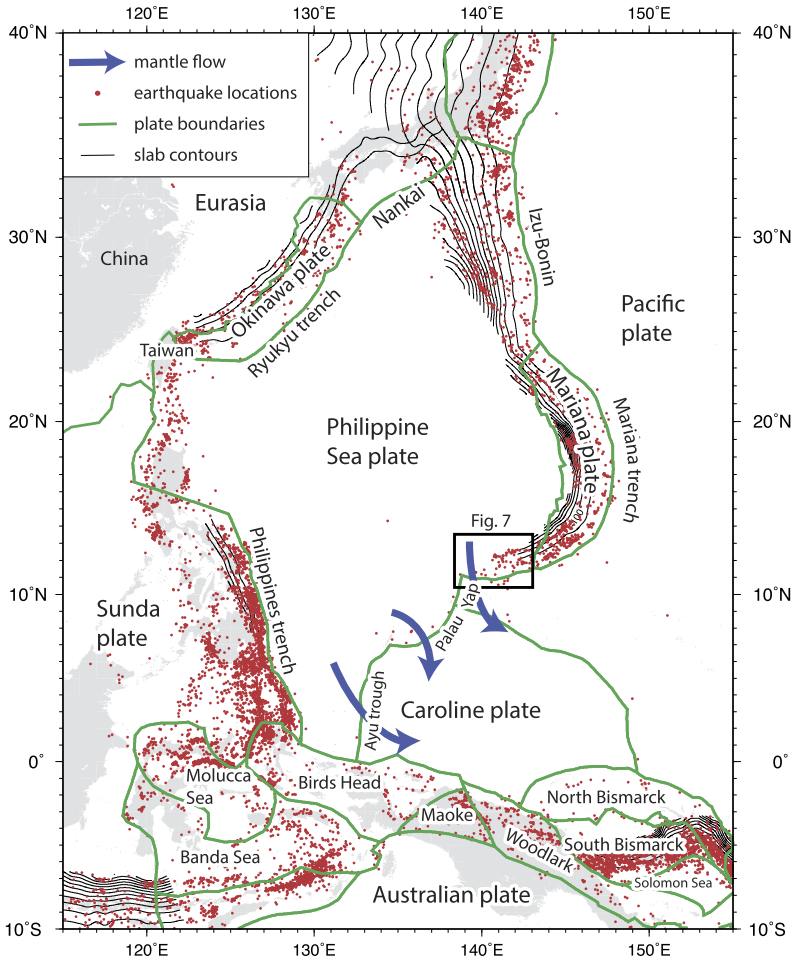

Fig. 6. Map of the Philippine Sea Plate illustrating possible slab gaps or tears. The red dots represent ISC epicenters for magnitudes ≥5 and for depths >33 km, from 1960 to present; and depict the Wadati–Benioff zones around the PSP. 50 km slab contours from the slab 1.0 model (Hayes et al., 2012) are also shown for reference. Apparent slab gaps occur at the southern end of the Philippine Sea plate (Ayu Trough), along the Yap and Palau Trenches, and at the southern end of the Mariana Trench. Note that although the Caroline Ridge may subduct aseismically underneath the Yap and Palau Trenches, no slab deeper than 40 km has been detected using local OBS arrays (Sato et al., 1997). Plate boundaries (thick green lines) are from Bird (2003). The black rectangle shows the expanded area of Fig. 7. (For interpretation of the references to color in this figure legend, the reader is referred to the web version of this article.)

ana Trough. To account for this addition to the Philippine Sea plate area, we subtract the growth rate of the Mariana backarc basin S_{MT} (km^2/Myr) from the above shrinkage rate S to estimate the total shrinking rate of PSP S_P (km^2/Myr), so that

$$S_P = S - S_{MT} \tag{2}$$

There is, however, no well-defined rotation pole for the Mariana Trough opening (Kato et al., 2003). To estimate the growth of the backarc basin, we can integrate its digitized area A_{MT} (i.e., 0.27×10^6 km^2) over time, that is

$$S_{MT} = dA_{MT}/dt \tag{3}$$

Assuming a backarc opening from ~5 to 10 Ma, we find that the Mariana Trough is growing at a rate of 27.3×10^3 km^2/Myr (digitized area integrated over 10 Ma) to 54.5×10^3 km^2/Myr (area integrated over 5 Ma). From Eq. (2), we find that PSP is shrinking at a rate S_P of about 237.4–210.2 $\times 10^3$ km^2/Myr. This forces low viscosity asthenosphere to escape from underneath the shrinking PSP.

Below, we investigate the occurrence of a slab gaps around PSP and, in particular, along the southern tip of the Mariana Trench, which provides pathways for escaping asthenosphere. Then, we use our new Hf–Nd isotopic ratios to investigate mantle provenance and further infer mantle flows in the southern Marianas.

7. Slab gaps and tears around the Philippine Sea and Mariana plates

We compiled earthquake locations (http://www.isc.ac.uk) from December 1960 to present with magnitudes >5 and hypocenters deeper than 33 km, and we used these to outline the seismic Wadati–Benioff zones of the circum-PSP region (Fig. 6) and, locally, the southern Mariana margin (Fig. 7). We also show interpolated slab contours from Hayes et al. (2012). The downgoing slab plunges steeply beneath the southern Mariana convergent margin, and most seismic events occur within the slab interior down to about 300 km depths (Fig. 7). Additionally, the Pacific plate subducting at the southwestern Mariana Trench loses teleseismic definition (Hayes et al., 2012), and the slab is short (<40 km depths; Sato et al., 1997) and narrow at the adjacent Yap Trench. These observations reveal a seismic gap beginning near the southwestern tip of the Mariana Trench and continuing south, which may reflect a slab gap (Figs. 6 and 7). Subduction at the Palau Trench transitions to divergence along the Ayu Trough, at the southern end of the Philippine Sea plate (Fig. 6). This may also provide an avenue for asthenospheric outflow, although the Caroline Ridge may subduct aseismically in the region (Fig. 6). This possible slab gap, along the southern end of the Mariana Trench (Fig. 7) and abutting the Caroline plate at the Yap and Palau Trenches and Ayu Trough

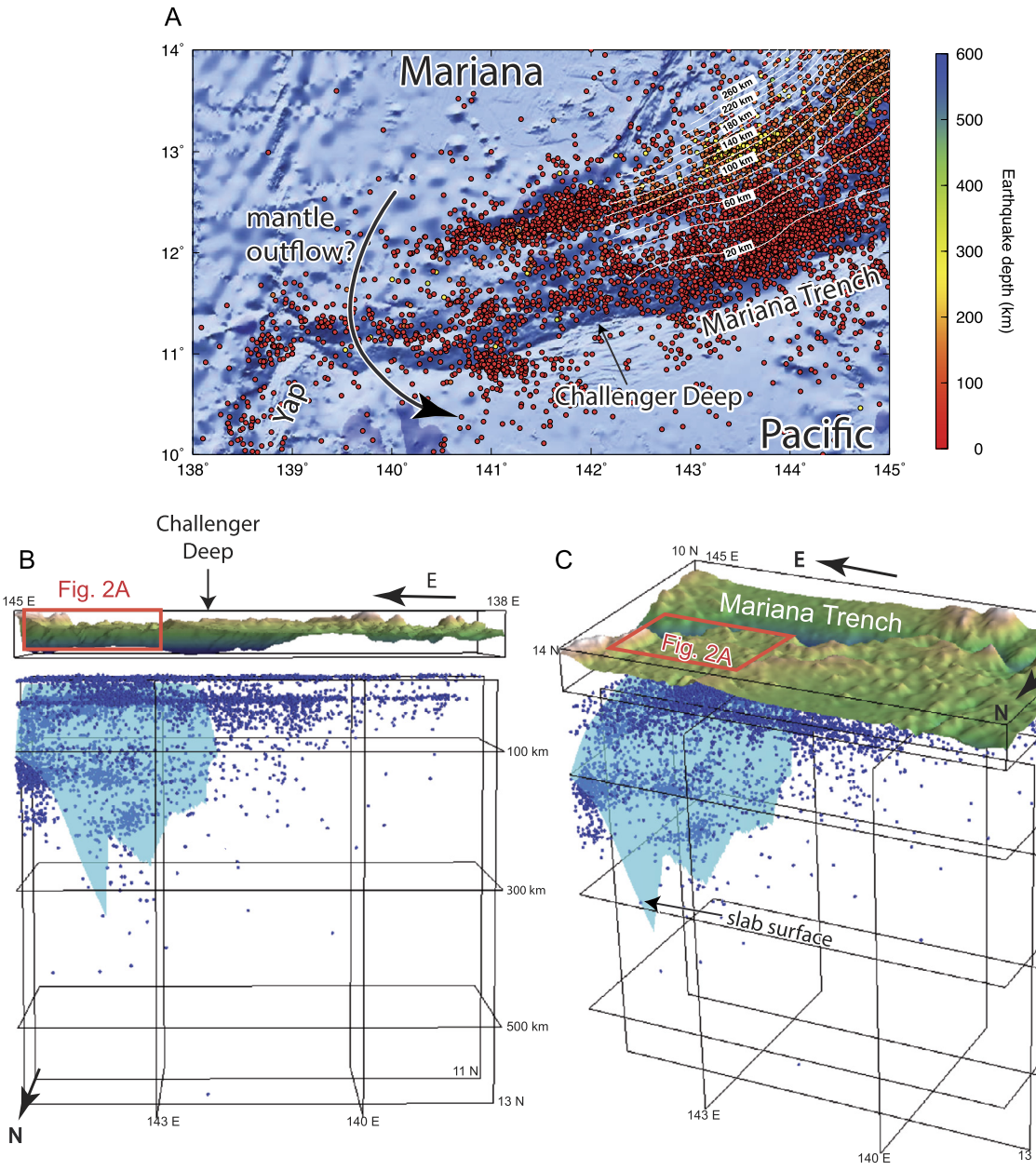

Fig. 7. Seismicity distribution along the Pacific plate subducting beneath the southern Mariana convergent margin. A) Bathymetric map showing the intra-slab seismicity. Earthquake hypocenters are marked by spheres colored from red to blue with increasing slab depths. Slab contours (white lines) are every 20 km. B, C) Three-dimensional visualization of seismicity distribution (blue spheres) along the downgoing Pacific plate. The slab surface (light blue field) is interpolated from the slab seismicity (Hayes et al., 2012). Seismicity distribution is viewed from the north in panel B and from the northwest in panel C. The red rectangle shows the expanded area of Fig. 2A. Lack of seismicity in the southwestern part of the downgoing Pacific plate suggests that the slab is ending in that region. (For interpretation of the references to color in this figure legend, the reader is referred to the web version of this article.)

(Fig. 6), could thus provide a major avenue for mantle outflow from a shrinking PSP, which is elsewhere surrounded by downgoing plates, thickened arc crust and continental margin crust.

8. Tracking mantle provenance using Hf–Nd isotopes

Combined Hf–Nd isotope systematics have widely been used as tracers of mantle flow as they can help discriminate the mantle origin of subduction zone magmas (e.g., Hickey-Vargas et al., 1995; Pearce et al., 1999). In the Western Pacific, the mantle source of Mariana arc and Mariana Trough backarc basin magmas has long been thought to have a predominantly Indian-type affinity. In contrast, the asthenospheric mantle flowing underneath the downgoing Pacific plate is thought to have a Pacific isotopic fingerprint (Fig. 1B–C). The present Indian–Pacific isotopic boundary is thought to roughly coincide with the current location of the Izu-Bonin–Mariana subduction zone (e.g., Hickey-Vargas et al., 1995; Klein et al., 1988; Pearce et al., 1999), although some deviations have been proposed (Miyazaki et al., 2015; Straub et al., 2009). Below, we use Hf–Nd systematics to evaluate whether the asthenosphere flowing beneath the southern Marianas comes from underneath the northern part of the Mariana Trough or elsewhere from beneath the PSP or from underneath the subducting Pacific plate.

8.1. Filtering the Hf–Nd isotopic ratios of the Southern Mariana lavas from their subduction influence

Combined Hf and Nd isotopic compositions of convergent margin lavas are considered to best preserve a record of their mantle source (Hickey-Vargas et al., 1995; Miyazaki et al., 2015), compared

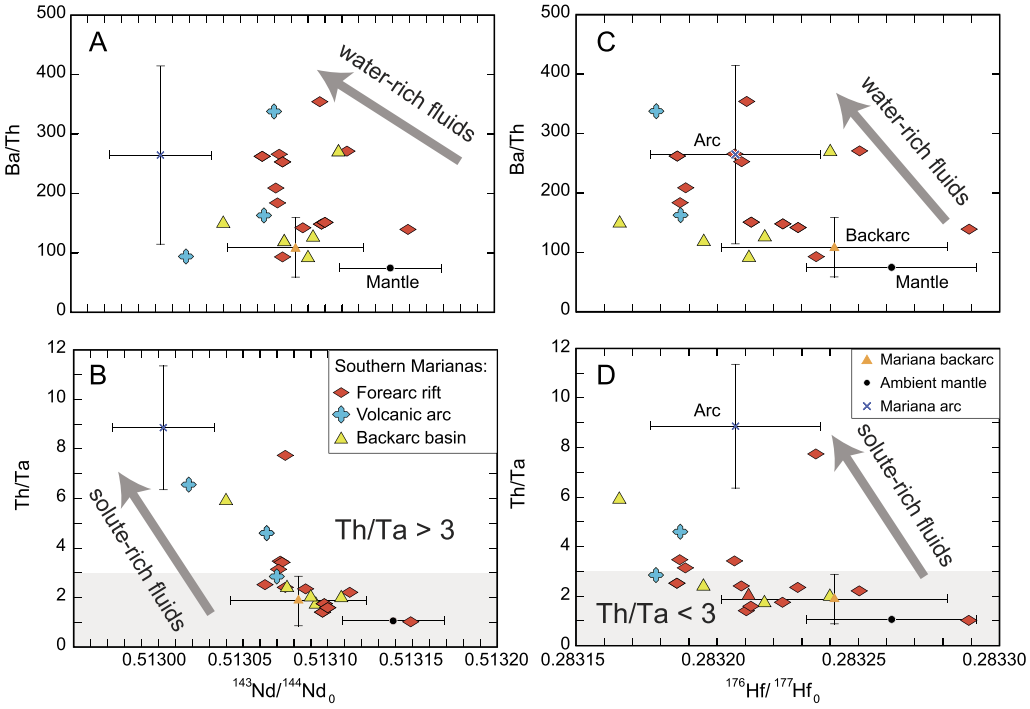

Fig. 8. Evaluating the role of the slab fluids on the mobility of Hf–Nd isotopic ratios. A, C) The Ba/Th ratio tracks the water-rich fluids released from the slab, and B, D) the Th/Ta ratio tracks the solute-rich melt released during sediment melting. The Hf–Nd isotopic composition of the southern Mariana lavas (gray symbols), and the averaged composition of the northern Mariana arc and backarc lavas (green symbols) systematically plot to the left of the ambient mantle. The correlation between the Hf–Nd composition of the lavas and the proxies for the slab fluids (i.e. Ba/Th and Th/Ta) implies that the subduction input may modify the Hf–Nd isotopic ratios of the lavas. Thus, the Hf–Nd isotopic composition of subduction zone lavas does not reflect the composition of their mantle source. Averages for the Mariana arc and backarc lavas and ambient mantle are reported with one standard deviation error bar. Details can be found in the supplementary Table B1-1.

to other isotopic tracers such as Pb and Sr, as they are relatively insensitive to the influence of aqueous fluids released from the subducting plate (Pearce et al., 1999; Woodhead et al., 2001, 2011). However, Nd and Hf isotopic ratios may be mobilized with the solute-rich fluids released during melting of subducting sediments (Woodhead et al., 2001, 2011), which may thus have compromised the original Hf–Nd isotopic composition of the mantle source of subduction zone lavas.

By filtering data (i.e., using samples with Th/Ta $<$ 3 and Ba/Nb $<$ 7) so as to exclude samples possessing a strong subduction signal (including slab-derived sediment melts), Woodhead et al. (2012) identified the composition of the pre-subduction mantle flowing beneath the Mariana Trough – which they termed '*ambient mantle*' (i.e., mantle without any subduction influence; Fig. 4A), after Todd et al. (2011). The subduction influence for the unfiltered Mariana lavas can be seen in the Hf–Nd isotope diagram (Fig. 4). The involvement of subduction components typically drives the original composition of the lavas toward lower Hf and Nd isotopic ratios (i.e., to the left in Fig. 4), so that lavas will plot into a region with greater 'Indian' mantle affinity. Filtering out such influences on convergent margin lavas is therefore critical before using them to assign mantle parentage. Below, we explore the effect of the slab-derived fluids on the Hf–Nd isotopic composition of the southern Mariana lavas.

8.2. Mobility of Hf–Nd isotopic ratios with water-rich fluids?

Although Hf and Nd are generally thought to be mobile only with mantle and sediment melts (Pearce et al., 1999; Woodhead et al., 2011), several studies question the immobility of Hf in water-rich, slab-derived fluids (Woodhead et al., 2001). Southern Mariana lavas are influenced to some extent by aqueous slab-derived fluids, which may drive their original mantle isotopic composition towards the Indian side in the Hf–Nd diagram (i.e., to the left in Fig. 4A). Therefore, it is conceivable that southern Mariana lavas may derive from melting of metasomatized Pacific mantle; and their apparent Indian affinity may reflect a subduction contribution to their mantle source. In the light of such possibilities, it is important to re-evaluate the nature of the mantle domains. Here, we attempt to do this by exploring the influence of the slab fluids on the Hf–Nd isotopic composition of their mantle source prior to any subduction influence.

Covariations of Hf and Nd isotopic ratios with proxies for aqueous slab fluids (i.e., Ba/Th; Pearce et al., 2005) suggest that the averaged isotopic composition of the Mariana arc and backarc lavas is shifted towards the left compared to the composition of the Mariana ambient mantle (Fig. 8). The involvement of subduction components (i.e., sediment melts and water-rich fluids) drives the original composition of the mantle (i.e., prior to any subduction input) toward lower Hf and Nd isotopic ratios (i.e., to the left in Nd–Hf isotope diagrams; Fig. 4A), so that the resulting lavas will plot in a region with greater 'Indian' mantle affinity. These observations suggest that Hf and Nd isotopic ratios of the lavas may be affected by the water-rich fluids, and they may have not preserved the original Hf–Nd isotopic composition of their mantle source (Fig. 4A). The southern Mariana lavas cannot, however, be filtered for their subduction influence (i.e., Th/Ta $<$ 3 and Ba/Nb $<$ 7) as in Woodhead et al. (2012), because all the lavas possess high Ba/Nb ratios (Ba/Nb $>$ 7; Table 1). To overcome this, we reconstruct the composition of the mantle source of southern Mariana lavas prior to any subduction contribution using simple mass balance calculations (Langmuir et al., 1978) as Pearce et al. (1999), that is:

$$C_M = C_{PM} \times f_{PM} + C_S \times f_S \quad (4)$$

$$R_M = \frac{C_{PM} \times R_{PM} \times f_{PM} - C_S \times R_S \times f_S}{C_{PM} \times f_{PM} + C_S \times f_S} \quad (5)$$

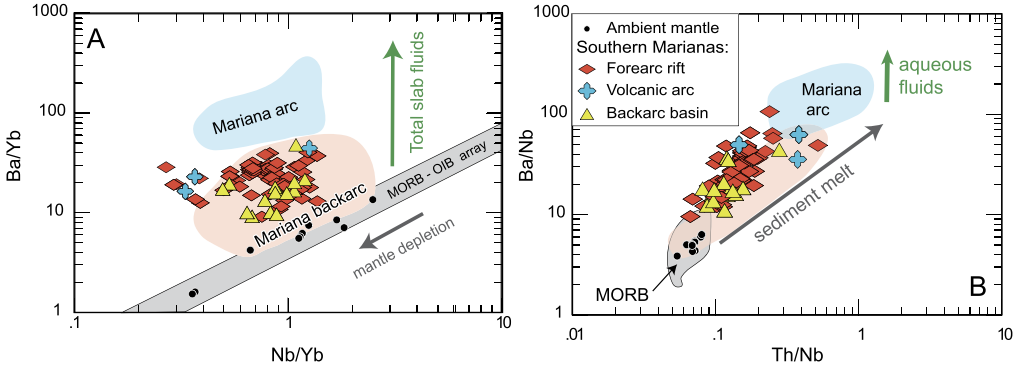

Fig. 9. Influence of the slab fluids on the Southern Mariana samples. A) Ba/Yb vs. Nb/Yb and B) Ba/Nb vs. Th/Nb diagrams of Pearce et al. (2005). The Southern Mariana lavas display lower, backarc-like Ba/Yb, Ba/Nb (i.e., proxies for the total subduction contribution) and Th/Nb ratios (i.e., proxy for the sediment melt input) than do the Mariana arc lavas, because they captured lower extent of sediment melt released during sinking of the slab. This support the notion that melting of the downgoing plate is minimal in that region. The MORB-OIB array was defined using the dataset of Jenner and O'Neill (2012). References can be found in Appendix D.

The original isotopic composition of the pre-subduction mantle R_{PM} is thus given by Eq. (6):

$$R_{PM} = \frac{(C_{PM} \times f_{PM} + C_S \times f_S) \times R_M - C_S \times R_S \times f_S}{C_{PM} \times f_{PM}} \quad (6)$$

f_S is the fraction (%) of total slab fluids, including the slab melts and the aqueous fluids, and f_{PM} is fraction (%) of pre-subduction mantle (i.e., $f_{PM} = 1 - f_S$). C_{PM} is the trace element composition (in ppm) of the pre-subduction mantle, C_M is the trace element content of the mantle wedge modified by the slab fluids (ppm), C_S is the trace element content of the total slab fluids (ppm), and C_L is the composition of the lavas (ppm). We consider that the lavas formed by 20% melting of the modified mantle (see supplementary material for details) in our mixing equations, which is taken as the averaged melting degree that produces the Mariana arc lavas (supplementary Fig. D1). R_L, R_S and R_M are respectively the isotopic compositions of the lavas, the total slab fluids and the modified mantle; and we consider that the isotopic composition of the lavas reflects that of their mantle source. The Pb isotopic ratios of southern Mariana lavas show that the Pacific plate plunging in that region has a Pacific flavor (Fig. 4C); and the Indian-type Caroline seamounts subducting along with the Pacific plate (Fig. 1B) have a minimal effect on the isotopic composition of the slab fluids. Hence, we use a 60:40 bulk mixture between the Pacific sediment and the altered oceanic crust (Vervoort et al., 2011) as an approximate to model the total slab fluid composition, as in Woodhead et al. (2012). Composition of the end-members used in our mixing calculations are reported in supplementary Table B1-2. Details of our calculations can be found in supplementary Table B1-3.

Using Eq. (6) to back-track the composition of the mantle source prior to any slab fluid contribution, we find that southern Mariana lavas could derive from a Pacific-type mantle if their subduction influence (i.e., the sediment melts and the water-rich fluids) is greater than 5%. In other words, a Pacific-type mantle that has interacted with at least 5% subduction component can produce Indian-type magmas, as the subduction influence shifts the Hf–Nd isotopic composition towards the left of the diagram (i.e., in the Indian side in Fig. 4A). Results of our mixing calculations for 5% and 10% of slab–fluid addition are depicted by the thin red lines in Fig. 4A; and the averaged Hf–Nd isotopic compositions of the reconstructed mantle source are represented by the red diamonds (see supplementary Table B1-2 for details). However, the Mariana arc lavas have generally captured less than 5% total slab fluids, as depicted by a thin black line in Fig. 4A. Because the Mariana arc lavas captured much higher extent of total slab fluids than do the southern Mariana lavas (Fig. 8 and 9), it is reasonable to consider that the southern Mariana lavas interacted with less than 5% total slab fluids. In such a scenario, the reconstructed Hf–Nd isotopic composition of the mantle source of the southern Mariana lavas is only slightly shifted towards the left of the ambient mantle array in Fig. 4A; and it plots within the Indian compositional field. Therefore, addition of less than 5% slab fluids to the mantle cannot shift the Hf–Nd isotopic composition of the mantle across the Indian–Pacific mantle boundary, so that Indian-type lavas must derive from an Indian-type mantle source.

Despite the fact that slab fluid contribution can modify the Hf–Nd isotopic composition of subduction-related lavas (Fig. 8), our mixing calculations show that addition of less than 5% total slab fluids has a minimal effect on the Hf–Nd isotopic composition of the southern Mariana lavas (Fig. 4A). Hence, we conclude that the southern Mariana lavas have likely preserved the original Indian fingerprint of their mantle source, which is compositionally similar to the Mariana ambient mantle defined by Woodhead et al. (2012).

8.3. An Indian mantle flow beneath the Southern Marianas

To ensure that southern Mariana lavas preserve their mantle source Hf–Nd isotopic composition, samples were filtered to emphasize those with minimal sediment input (i.e., Th/Ta < 3) as in Woodhead et al. (2012). Six samples were thus filtered out (i.e., Th/Ta range from 1.02 to 7.74; Table 1), as depicted by the unfilled symbols in Fig. 4A. The southern Mariana lavas encompass the known Hf–Nd compositional spectrum of the Mariana ambient mantle of Woodhead et al. (2012). Such observations further suggest that their sediment contributions are invariably small, and this filtering does not affect the compositional variability of Hf–Nd isotopic ratios of these lavas. These observations are consistent with the notion that both Hf and Nd isotopic ratios of southern Mariana lavas are insensitive to the influence of fluids derived from the subducting plate. They thus preserve a better record of their mantle source compared to isotopic tracers such as Pb and Sr (Pearce et al., 1999), which cannot be used to infer their original mantle composition. We conclude that the southern Mariana lavas effectively captured their original mantle Nd–Hf compositional variations. The broad spectrum in Hf–Nd of the southern Mariana lavas, within a localized region, reflects mantle heterogeneities at various scales.

The fact that the southern Mariana lavas have Hf–Nd isotopic characteristics similar to the previously identified Mariana ambient mantle (Fig. 4) implies that an Indian-type mantle is flowing beneath the region. Opening of the Mariana Trough at ~5–10 Ma enabled Indian-type ambient mantle to flow south- or eastward into the rapidly-extending southern Mariana convergent margin (i.e., from the backarc basin spreading center towards the trench).

Using geodetic data, we have demonstrated that the PSP is shrinking (Fig. 5 and Section 6), and the underlying asthenosphere is thus progressively squeezed out to escape through gaps in the subducted Pacific plate (Fig. 6). Hence, we conclude that the mantle flows around the slab tear or gap are in the opposite sense as generally assumed by slab-driven mantle flow models (Fig. 2B) (Schellart et al., 2007; Strak and Schellart, 2014). These observations are consistent with our new geochemical results, indicating that Mariana Trough ambient mantle is flowing outward and provides a supply of fresh, undepleted asthenosphere beneath the southern Marianas. The rapid slab advance may have, therefore, facilitated forearc rifting near the southern Mariana Trench.

9. Conclusions

Our new Hf–Nd isotopic data indicate that southern Mariana asthenosphere has an Indian flavor, similar to the ambient mantle flowing beneath the Mariana Trough. This finding further implies that PSP asthenosphere flows outward to feed the southern Mariana lavas. Our interpretation is consistent with geodetic data, which indicates that the IBM trenches are advancing towards Eurasia and the PSP shrinking, requiring asthenospheric outflow. Mariana Trough ambient mantle may thus escape through the slab tear or gap to accommodate plate motions, instead of flowing in, as proposed by most slab-motion driven mantle flow models. Outflow of asthenospheric mantle underneath the Philippine Sea plate could be further evidenced by drilling samples from active seamounts erupting onto the Pacific plate in the vicinity of the southern Mariana Trench, as well as in the downgoing plates subducting underneath the Philippines Sea plate (i.e., Yangtze and Caroline plates) (Fig. 6), by further examining the isotopic composition of recently erupted arc lavas, by studying young lavas of the Ayu Trough, and by tracking mantle flow patterns using $^{3}He/^{4}He$ geochemical mapping.

Acknowledgements

We thank crews of the R/V Yokosuka and the R/V Thomas Thompson for their efforts. This study was conducted under the special use permit #12541-12001 of US Fish and Wildlife Service for activities in the Mariana Trench Marine National Monument. We thank US Fish and Wildlife Service for approval of our study in the monument. We thank Roland Maas for assistance with the isotope analyses at Melbourne, and J. Gill (USCS), C. Kincaid (URI), C. Chauvel (ISTERRE), J. Pearce (Cardiff University) and Tiffany Barry (University of Leicester) for their insightful comments, as well as K. Kelley (URI) for sharing samples and comments. We also thank editor An Yin for handling the manuscript, and two anonymous reviewers who helped improve the manuscript. This research was supported by US National Science Foundation grants 0961352 to RJS and 0961811 to FM. This is UTD Geosciences contribution #1304.

Appendix A. Supplementary material

Supplementary material related to this article can be found online at http://dx.doi.org/10.1016/j.epsl.2017.08.022.

References

Alvarez, W., 1982. Geological evidence for the geographical pattern of mantle return flow and the driving mechanism of plate tectonics. J. Geophys. Res., Solid Earth 87 (B8), 6697–6710.

Alvarez, W., 2001. Eastbound sublithosphere mantle flow through the Caribbean gap and its relevance to the continental undertow hypothesis. Terra Nova 13 (5), 333–337.

Bird, P., 2003. An updated digital model of plate boundaries. Geochem. Geophys. Geosyst. 4 (3), 1027. http://dx.doi.org/10.1029/2001GC000252.

Brounce, M., Kelley, K., Cottrell, E., 2014. Variations in $Fe^{3+}/\Sigma Fe$ of Mariana Arc basalts and mantle wedge fO_2. J. Petrol. 55 (12), 2513–2536.

Brounce, M.N., Kelley, K.A., Stern, R.J., Martinez, F., Cottrell, E., 2016. The Fina Nagu Volcanic complex: unusual submarine arc volcanism in the rapidly deforming southern Mariana margin. Geochem. Geophys. Geosyst. 17, 4078–4091. http://dx.doi.org/10.1002/2016GC006457.

Carlson, R.L., Melia, P.J., 1984. Subduction hinge migration. Tectonophysics 102 (1), 399–411.

Carlson, R.L., Mortera-Gutiérrez, C.A., 1990. Subduction hinge migration along The Izu-Bonin–Mariana arc. Tectonophysics 181 (1), 331–344.

Caulfield, J.T., Turner, S.P., Smith, I.E.M., Cooper, L.B., Jenner, G.A., 2012. Magma evolution in the primitive, intra-oceanic Tonga Arc: petrogenesis of basaltic Andesites at Tofua Volcano. J. Petrol. 53 (6), 1197–1230.

Conrad, C.P., Lithgow-Bertelloni, C., 2002. How Mantle slabs drive plate tectonics. Science 298 (5591), 207–209.

Dvorkin, J., Nur, A., Mavko, G., Ben-Avraham, Z., 1993. Narrow subducting slabs and the origin of backarc basins. Tectonophysics 227, 63–79.

Elsasser, W.M., 1971. Two-layer model of upper-mantle circulation. J. Geophys. Res. 76 (20), 4744–4753.

Fryer, P., Becker, N., Appelgate, B., Martinez, F., Edwards, M., Fryer, G., 2003. Why is the Challenger Deep so deep? Earth Planet. Sci. Lett. 211, 259–269.

Fryer, P., Mottl, M., Johnson, L., Haggerty, J., Phipps, S., Maekawa, H., 1995. Serpentine bodies in the forearcs of western pacific convergent margins: origin and associated fluids. In: Active Margins and Marginal Basins of the Western Pacific. American Geophysical Union, pp. 259–279.

Govers, R., Wortel, M.J.R., 2005. Lithosphere tearing at STEP faults: response to edges of subduction zones. Earth Planet. Sci. Lett. 236 (1–2), 505–523.

Gvirtzman, Z., Stern, R.J., 2004. Bathymetry of Mariana trench-arc system and formation of the Challenger Deep as a consequence of weak plate coupling. Tectonics 23 (2), TC2011. http://dx.doi.org/10.1029/2003tc001581.

Hayes, G.P., Wald, D.J., Johnson, R.L., 2012. Slab1.0: a three-dimensional model of global subduction zone geometries. J. Geophys. Res., Solid Earth 117 (B1), B01302. http://dx.doi.org/10.01029/02011JB008524.

Hickey-Vargas, R., Hergt, J.M., Spadea, P., 1995. The Indian Ocean-type isotopic signature in western Pacific marginal basins: origin and significance. In: Taylor, B., Natland, J. (Eds.), Active Margins and Marginal Basins of the Western Pacific. American Geophysical Union, Washington, D.C., pp. 175–197.

Hussong, D., Uyeda, S., 1982. Tectonic processes and the history of the Mariana arc: a synthesis of the results of Deep Sea Drilling Project Leg 60. In: Hussong, D., Uyeda, S. (Eds.), Initial Report Deep Sea Drilling Project, vol. 60. U.S. Government Printing Office, Washington, D.C., pp. 909–929.

Hyndman, R.D., Peacock, S.M., 2003. Serpentinization of the forearc mantle. Earth Planet. Sci. Lett. 212 (3–4), 417–432.

Jenner, F.E., O'Neill, H.S.C., 2012. Analysis of 60 elements in 616 ocean floor basaltic glasses. Geochem. Geophys. Geosyst. 13, Q02005. http://dx.doi.org/10.01029/02011gc004009.

Kato, T., Beavan, J., Matsushima, T., Kotake, Y., Camacho, J.T., Nakao, S., 2003. Geodetic evidence of backarc spreading in the Mariana Trough. Geophys. Res. Lett. 30. http://dx.doi.org/10.1029/2002GL016757.

Kincaid, C., Griffiths, R.W., 2003. Laboratory models of the thermal evolution of the mantle during rollback subduction. Nature 425 (4), 58–62.

Klein, E.M., Langmuir, C.H., Zindler, A., Staudigel, H., Hamelin, B., 1988. Isotope evidence of a mantle convection boundary at the Australian–Antarctic discordance. Nature 333 (6174), 623–629.

Kobayashi, K., 2004. Origin of the Palau and Yap trench–arc systems. Geophys. J. Int. 157 (3), 1303–1315.

Langmuir, C.H., Vocke, R.D., Hanson, G.N., Hart, S.R., 1978. A general mixing equation with applications to Icelandic basalts. Earth Planet. Sci. Lett. 37 (3), 380–392.

Maas, R., Kamenetsky, M.B., Sobolev, A.V., Kamenetsky, V.S., Sobolev, N.V., 2005. Sr, Nd, and Pb isotope evidence for a mantle origin of alkali chlorides and carbonates in the Udachnaya kimberlite, Siberia. Geology 33 (7), 549–552.

Millen, D.W., Hamburger, M.W., 1998. Seismological evidence for tearing of the Pacific plate at the northern termination of the Tonga subduction zone. Geology 26 (7), 659–662.

Miyazaki, T., Kimura, J.-I., Senda, R., Vaglarov, B.N.S., Chang, Q., Takahashi, T., Hirahara, Y., Hauff, F., Hayasaka, Y., Sano, S., Shimoda, G., Ishizuka, O., Kawabata, H., Hirano, N., Machida, S., Ishii, T., Tani, K., Yoshida, T., 2015. Missing western half of the Pacific Plate: geochemical nature of the Izanagi–Pacific Ridge interaction with a stationary boundary between the Indian and Pacific mantles. Geochem. Geophys. Geosyst. 16 (9), 3309–3332.

Molnar, P., Atwater, T., 1978. Interarc spreading and Cordilleran tectonics as alternates related to the age of subducted oceanic lithosphere. Earth Planet. Sci. Lett. 41 (3), 330–340.

Ohara, Y., Ishii, T., 1998. Peridotites from the southern Mariana forearc: heterogeneous fluid supply in mantle wedge. Isl. Arc 7 (3), 541–558.

Ohara, Y., Reagan, M.K., Fujikura, K., Watanabe, H., Michibayashi, K., Ishii, T., Stern, R.J., Pujana, I., Martinez, F., Girard, G., Ribeiro, J., Brounce, M., Komori, N., Kino, M., 2012. A serpentinite-hosted ecosystem in the Southern Mariana Forearc. Proc. Natl. Acad. Sci. 109 (8). http://dx.doi.org/10.1073/pnas.1112005109.

Okino, K., Ohara, Y., Kasuga, S., Kato, Y., 1999. The Philippine Sea: a new survey results reveal the structure and history of the marginal basins. Geophys. Res. Lett. 26 (15), 2287–2290.

Pearce, J.A., Kempton, P.D., Nowell, G.M., Noble, S.R., 1999. Hf–Nd element and isotope perspective on the nature and provenance of mantle and subduction components in western Pacific arc-basin systems. J. Petrol. 40 (11), 1579–1611.

Pearce, J.A., Stern, R.J., Bloomer, S.H., Fryer, P., 2005. Geochemical mapping of the Mariana arc-basin system: implications for the nature and distribution of subduction components. Geochem. Geophys. Geosyst. 6 (7), Q07006. http://dx.doi.org/10.01029/02004GC000895.

Peccerillo, A., Taylor, S.R., 1976. Geochemistry of Eocene calcalkaline volcanic rocks from the Kastamonu Area, Northern Turkey. Contrib. Mineral. Petrol. 58, 63–81.

Ribeiro, J., Stern, R.J., Kelley, K., Martinez, F., Ishizuka, O., Manton, W.I., Ohara, Y., 2013a. Nature and distribution of the slab-derived fluids and the mantle source along the Southeast Mariana Forearc Rift. Geochem. Geophys. Geosyst. 14 (10), 4585–4607. http://dx.doi.org/10.1002/ggge.20244.

Ribeiro, J., Stern, R.J., Martinez, F., Ishizuka, O., Merle, S.G., Kelley, K.A., Anthony, E.Y., Ren, M., Ohara, Y., Reagan, M., Girard, G., Bloomer, S.H., 2013b. Geodynamic evolution of a forearc rift in the southernmost Mariana Arc. Isl. Arc 22, 453–476.

Ribeiro, J.M., Stern, R.J., Kelley, K., Shaw, A., Martinez, F., Ohara, Y., 2015. Composition of the slab-derived fluids released beneath the Mariana forearc: evidence for shallow dehydration of the subducting plate. Earth Planet. Sci. Lett. 418, 136–148. http://dx.doi.org/10.1016/j.epsl.2015.1002.1018.

Roeder, D., 1977. Philippine arc system—collision or flipped subduction zones? Geology 5 (4), 203–206.

Sato, T., Kasahara, J., Katao, H., Tomiyama, N., Mochizuki, K., Koresawa, S., 1997. Seismic observations at the Yap Islands and the northern Yap Trench. Tectonophysics 271 (3–4), 285–294.

Schellart, W.P., Freeman, J., Stegman, D.R., Moresi, L., May, D., 2007. Evolution and diversity of subduction zones controlled by slab width. Nature 446 (7133), 308–311.

Stern, R.J., Ren, M., Kelley, K.A., Ohara, Y., Martinez, F., Bloomer, S.H., 2014. Basaltic volcaniclastics from the Challenger Deep forearc segment, Mariana convergent margin: implications for tectonics and magmatism of the southernmost Izu-Bonin–Mariana arc. Isl. Arc 23 (4), 368–382.

Stern, R.J., Tamura, Y., Masuda, H., Fryer, P., Martinez, F., Ishizuka, O., Bloomer, S.H., 2013. How the Mariana Volcanic Arc ends in the south. Isl. Arc 22, 133–148.

Strak, V., Schellart, W.P., 2014. Evolution of 3-D subduction-induced mantle flow around lateral slab edges in analogue models of free subduction analysed by stereoscopic particle image velocimetry technique. Earth Planet. Sci. Lett. 403, 368–379.

Straub, S.M., Goldstein, S.L., Class, C., Schmidt, A., 2009. Mid-ocean-ridge basalt of Indian type in the northwest Pacific Ocean basin. Nat. Geosci. 2 (4), 286–289.

Sun, S.S., McDonough, W.F., 1989. Chemical and isotopic systemics of ocean basalt: implications for mantle composition and processes. In: Saunders, A.D., Norry, M.J. (Eds.), Magmatism in the Ocean Basins. Geol. Soc. (Lond.) Spec. Publ. 42, 313–345.

Suppe, J., 1984. Kinematics of arc-continent collision, flipping of subduction, and backarc spreading near Taiwan. Mem. Geol. Soc. China 6, 21–33.

Todd, E., Gill, J.B., Wysoczanski, R.J., Hergt, J., Wright, I.C., Leybourne, M.I., Mortimer, N., 2011. Hf isotopic evidence for small-scale heterogeneity in the mode of mantle wedge enrichment: Southern Havre Trough and South Fiji Basin back arcs. Geochem. Geophys. Geosyst. 12 (9), Q09011. http://dx.doi.org/10.01029/02011GC003683.

Turner, S., Hawkesworth, C., 1998. Using geochemistry to map mantle flow beneath the Lau Basin. Geology, 1019–1022.

Vervoort, J.D., Plank, T., Prytulak, J., 2011. The Hf–Nd isotopic composition of marine sediments. Geochim. Cosmochim. Acta 75 (20), 5903–5926.

Woodhead, J., Hergt, J.M., Greig, A., Edwards, L., 2011. Subduction zone Hf-anomalies: Mantle messenger, melting artefact or crustal process? Earth Planet. Sci. Lett. 304 (1–2), 231–239.

Woodhead, J.D., Hergt, J.M., Davidson, J.P., Eggins, S.M., 2001. Hafnium isotope evidence for 'conservative' element mobility during subduction zone processes. Earth Planet. Sci. Lett. 192 (3), 331–346.

Woodhead, J.D., Stern, R.J., Pearce, J.A., Hergt, J.M., Vervoort, J., 2012. Hf–Nd isotope variation in Mariana Trough basalts: the importance of "ambient mantle" in the interpretation of subduction zone magmas. Geology 40 (6), 539–542.